Nonlinear viscoelastic response of elastomers: Experiments, parameter identification and numerical simulation

A.F.M.S. Amin*, M.S. Alam**, Y. Okui***

* MSc. Engg. (Civil), Dept. of Civil and Environmental Eng, Saitama University, Urawa-shi, Saitama 338-0824
** Graduate Student, Dept. of Civil and Environmental Eng, Saitama University, Urawa-shi, Saitama 338-0824
***Dr. Eng., Associate Professor, Dept. of Civil and Environmental Eng, Saitama University, Urawa-shi, Saitama 338-0824

An experimental scheme is proposed to characterize the viscoelastic property of elastomers described by equilibrium response, instantaneous response and viscosity effect. The difficulties of directly applying infinitely fast or slow loading rate on this highly viscous material to obtain equilibrium and instantaneous responses and thereby to identify the nonlinear elastic parameters were overcome. To do this, experimental results were extrapolated and a modified hyperelasticity model was used. The hyperelasticity model was incorporated in a finite deformation rate-dependent model structure. The proposed scheme was applied on two different kinds of elastomers. Numerical simulation of test results followed by sensitivity studies verified the adequacy and robustness of the proposed scheme.

Key Words: Equilibrium response, instantaneous response, viscoelasticity, elastomers

1. Introduction

Apart from the traditional uses of elastomers in structural components like seals between tunnel segments and shock absorbers, the materials of this range are now also widely used in base isolation devices for protecting the structures from earthquakes. For such specific end use, high damping rubbers with the better energy absorption property have also been developed[1]. The mechanical behavior of all these materials is dominated by nonlinear rate-dependent elastic response. In addition, when subjected to cyclic loading, typical hysteresis and permanent set also appear. These two effects are specially more pronounced in high damping rubber. Hence, to reproduce the mechanical behavior of elastomers under cyclic loading, there is a necessity to develop a constitutive model that will be capable of simulating rate-dependent nonlinear response including hysteresis and permanent set. Although the final goal of this research is to develop a constitutive model representing all these aspects, the scope of this paper is restricted to the nonlinear viscoelastic behavior as the first step.

The rate-dependent responses obtained from a typical viscoelastic solid are schematically presented in Fig. 1. When a viscoelastic solid is loaded at an infinitely slow rate, the stress-strain curve follows the E-E' path. This behavior is called the equilibrium response. On the other hand, in case of an infinitely fast loading rate, the response takes the I-I' path. Such a response is known as the instantaneous response.

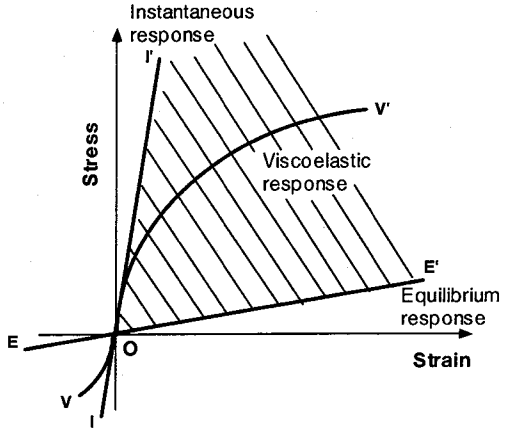

Figure 1. Typical responses from a viscoelastic solid.

Both equilibrium and instantaneous responses are elastic responses and the domain of viscosity lies between these two states[2]. Thus, elastic parameters determine the boundary of the domain where viscosity effects come into play. The area of the domain is directly related to the extent of material viscosity. In this context, one of the ways of developing a physically meaningful constitutive model is to include parameters that directly express the instantaneous and equilibrium behavior of the material. However, specially in case of highly viscous elastomeric materials, there are experimental limitations in applying infinitely slow and fast loading on a specimen to arrive at the equilibrium and instantaneous states respectively. Accordingly, most of the previous constitutive models include parameters to represent viscoelastic response without making any reference to instantaneous and equilibrium behavior of the material. On the other hand, even though the constitutive model contains the parameters to express the equilibrium and the instantaneous responses, these are estimated by numerical trials[3),4)] on the basis of data of the experiments carried out at the middle of viscous domain. The parameters identified in this way, however, lose the physical meaning.

With this background, we propose a parameter identification scheme to identify the parameters for instantaneous and equilibrium response from the experimental data. Although the scheme is applicable to both tensile and compressive loading, in this paper, the behavior under compression was investigated. The scheme was applied on two different types of elastomers to observe the fundamental viscoelastic behavior of each material under compression and thereby to check the applicability of the proposed scheme under varied material types. In this course, a finite deformation viscoelasticity model was considered for determining the material parameters from the experimental data. Numerical simulation results from the model using the identified parameters were compared with experimental data to verify the adequacy of the proposed scheme. Finally, a sensitivity study was carried out to discuss the robustness of the proposed scheme.

2. Experimental observation

The proposed experimental scheme to characterize the viscoelastic properties of elastomers comprises of a multi-step relaxation test, monotonic compression tests and simple relaxation tests. All the tests were carried out on two types of materials. The following sections present the details of the experiments and the inferences observed thereon.

2.1 Specimens

Two different kinds of elastomers namely 'Specimen-I' and 'Specimen-II' were chosen for the present study. Specimen-I is an elastomer for general-purpose use. The Specimen-II was manufactured in Yokohama Rubber Co. and it complies with G10 natural rubber specification for bridge bearings.

Both specimens differ each other from micro-structural point of view. Figure 2 shows the comparative microstructure of the specimens as visualized from scanning electron microscope (SEM) observation. The observation was made in a Jeol JSM 5600LV machine. The SEM images illustrate a void dominated microstructure of Specimen-I in contrast to the Specimen-II, where the occurrence of voids is rare.

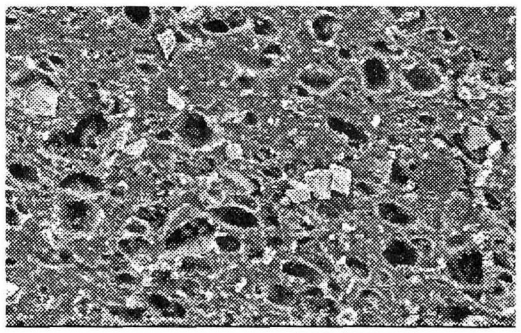

(a)

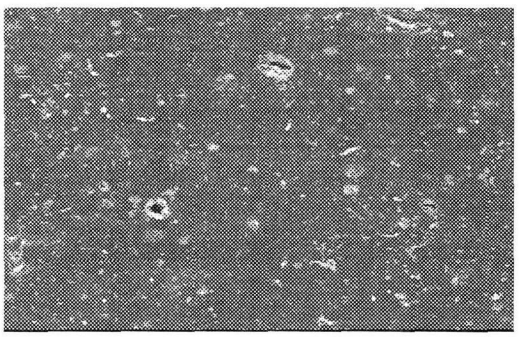

(b)

Figure 2. Micro-graphs of (a) Specimen-I; (b) Specimen-II.

2.2 Experimental set-up

Cubic blocks of Specimen-I (50mm on each side) and cylindrical blocks of Specimen-II (Height: 39 mm, Diameter: 49 mm) were tested at room temperature in a computer-controlled servo-hydraulic testing machine using Shimadzu servo-pulser 4800. In order to cut the friction between the sample and the loading plates, polypropylene films with lubricant on top and bottom of the sample were used. The axial force and the displacements were recorded

using a personal computer. In this context, the applied vertical displacement and the corresponding axial force of a loaded specimen were obtained from the servo-pulser output. The lateral displacement of the specimen was measured using a laser transducer (Ono Sokki LD-1110M-020). The measurement was taken at the midpoint of the specimen surface. However, due to very large applied vertical displacement (resulting up to 50% compressive strain), the midpoint of the specimen surface on deformation shifts significantly in vertical plane from its initial position. To overcome this problem and to catch the midpoint of the deformed specimen in vertical plane, a special type of jig using a boom device was used to move the laser transducer at a rate synchronized with the applied strain rate. Figure 3 shows the details of the experimental set-up.

In addition to direct measurement, lateral displacement of the specimen was also calculated from the measured vertical displacement and using assumptions of incompressibility and homogeneous deformation of the specimens. The lateral displacements obtained by using these two approaches were found to be within 2% of each other indicating the validity of the assumptions. In this situation, the applied stretch (i.e. 1+dL/L, where L is the undeformed length) and the Cauchy stress (true stress) for each test as presented in the following sections were calculated under the assumptions of homogeneous deformation and incompressibility of the specimens.

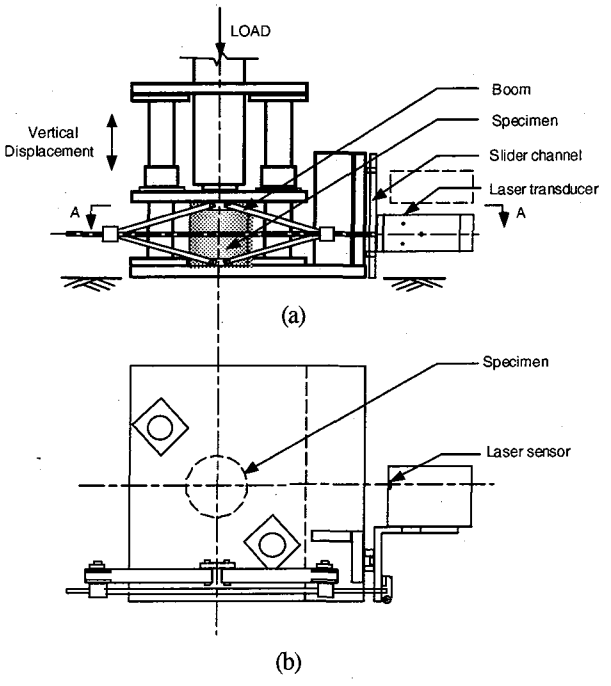

Figure 3. Experimental set-up. (a) Elevation; (b) Section A-A.

2.3 Pre-loading

Prior to actual experiment, all virgin specimens were subjected to a specified pre-loading sequence. The objective of the pre-loading was to obtain a stable state of the material by removing the Mullins softening effect[5] from other inelastic behavior. In the pre-loading, each virgin specimen was subjected to cyclic uniaxial compressive loading for 5 cycles with a strain rate of 0.01/s.

Figure 4 presents the time history of the applied stretch and stress-stretch relation in a pre-loading test for Specimen-I and Specimen-II. The softening behavior in the first loading cycle, known as the Mullins effect, is evident from the figure. In Specimen-I, the softening behavior is more pronounced than that in the Specimen-II. Both specimens showed a repeatable stress-stretch response after passing 2-3 loading cycles indicating the removal of the Mullins effect. However, the Mullins softening effect in a specimen recovers slowly with time. It is known as the 're-healing effect'[6]. To keep this re-healing effect to a constant amount for each specimen, in each test described in the following sections, a constant 20 min time interval was maintained between the pre-loading and the actual test. Apart from the Mullins effect, the typical strain-hardening feature of elastomers at higher strain level is more visible in Specimen-I than that in the Specimen-II after the first cycle of pre-loading.

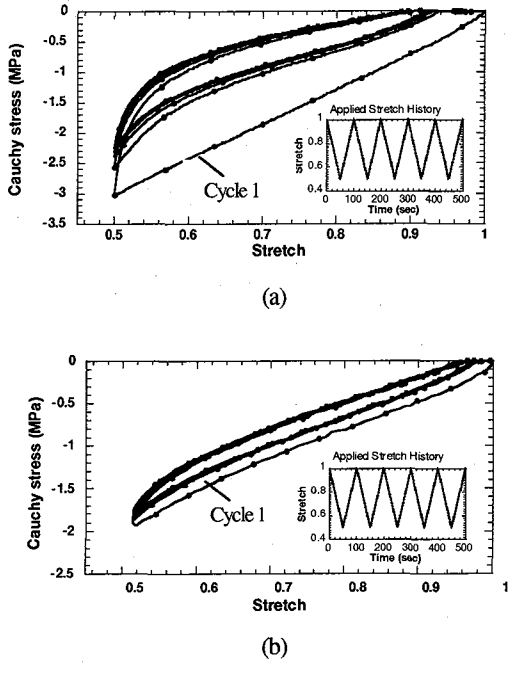

Figure 4. Applied stretch history and stretch-stress response observed in pre-loading. (a) Specimen-I (b) Specimen-II.

2.4 Multi-step relaxation test

A multi-step relaxation test was carried out to identify parameters for equilibrium response. In theory, the equilibrium response is obtained when a material is loaded at an infinitely slow rate. However, in case of highly viscous materials like elastomers, it is quite difficult to specify a loading rate that will be slow enough to rule out the viscosity effects. Thus it needs a number of uniaxial test trials. To address this problem, we employ multi-step relaxation test over the considered stretch range. In the present study, Specimen-I and Specimen-II were tested up to 0.55 and 0.5 stretch levels respectively. Figure 5 presents the applied stretch and obtained stress histories of the tests. It is seen that at the end of each relaxation interval of 10 min duration, each stress history converges to an almost constant state in both specimens. Although an equilibrium state can be achieved only in an asymptotic sense, the stress states indicate the neighborhood of the equilibrium states. We regard these stress states as the equilibrium states at respective stretch levels.

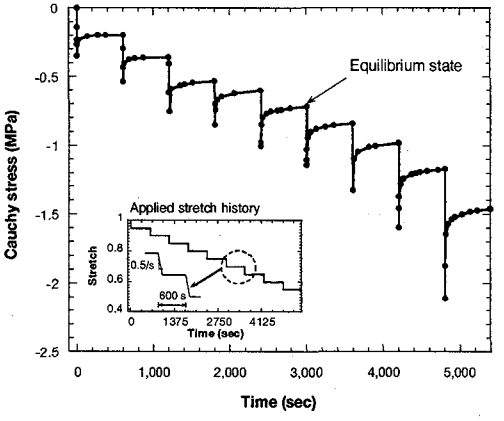

(a)

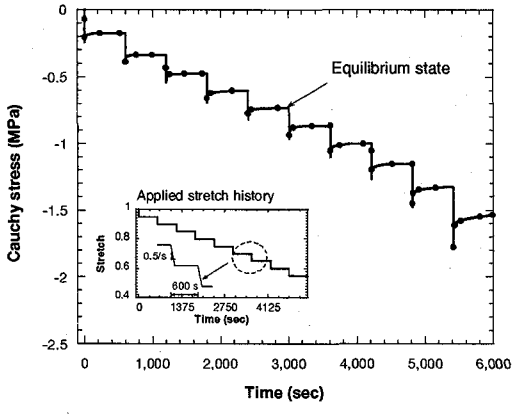

(b)

Figure 5. Applied stretch history and stretch-stress response observed in multi-step relaxation test. (a) Specimen-I (b) Specimen-II.

2.5 Monotonic compression test

The instantaneous elastic response of a solid is ideally obtained when the material is loaded at infinitely fast rate. From an experimental point of view, however, there is a finite maximum value of stroke rate for any displacement controlled loading device. Although, the use of a smaller specimen dimension in the loading direction can increase the loading rate on a specimen, the reduced aspect ratio of the specimen increases the boundary effects on the other turn. In this context, to find a method for estimating the instantaneous response, a series of monotonic compression tests was carried out. The tests were carried out at different constant strain-rates up to 0.5 stretch level. In the test series, a number of constant strain-rate cases within the range of 0.001/s to 0.96/s were considered.

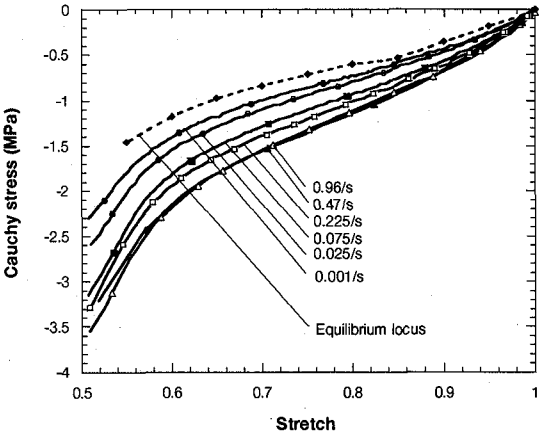

(a)

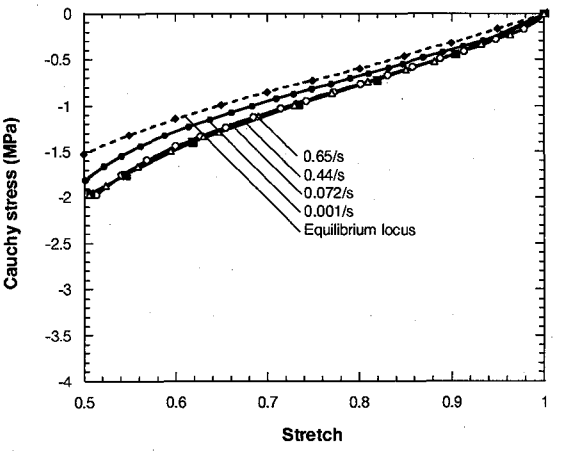

(b)

Figure 6. Comparison of monotonic compression test stretch-stress responses at different strain rates along with the equilibrium locus. (a) Specimen-I (b) Specimen-II.

Figure 6 shows the rate-dependent stress-stretch responses observed in six strain rate cases for Specimen-I and four strain rate cases for Specimen-II. A comparison of the curves of different strain rate cases in each specimen shows that with increasing strain-rate, the stresses increase due to viscosity effect. At higher strain rates, however, a diminishing trend in the increase of stress response was observed indicating the approach of an instantaneous state in both specimens. In this context, the stress response of Specimen-I obtained at and over 0.47/s strain rate can be considered as the neighborhood of instantaneous state boundary of the viscous domain (Fig. 1). In Specimen-II, the corresponding strain rate is 0.072/s.

To get a clearer picture of the viscous domain, the equilibrium loci obtained from Section 2.4 were compared here with different strain rate cases. The locus plotted in Fig. 6 represents the equilibrium state boundary of the viscous domain (Fig. 1) for each material. Comparisons between Figs. 6a and 6b shows that the equilibrium loci estimated for both specimens are comparable. However, the stress response of Specimen-II at faster strain rates is much lower than that of Specimen-I. This results in a much smaller viscous domain for Specimen-II characterizing low viscosity.

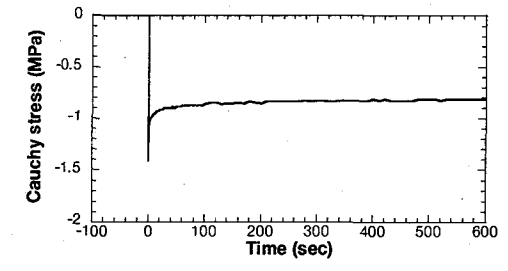

(a)

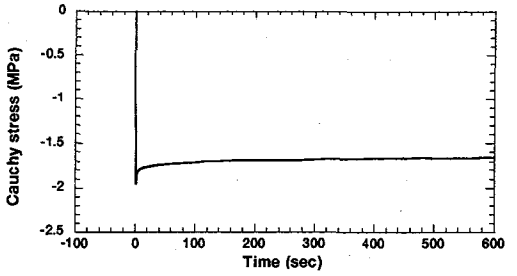

(b)

Figure 7. Stress history obtained from simple relaxation test. (a) Specimen-I (b) Specimen-II.

2.6 Simple relaxation test

The multi-step relaxation test and monotonic compression tests described in Sections 2.4 and 2.5 have made it possible to estimate the instantaneous and equilibrium responses thus defining the boundary of the viscous domain. The remaining problem is in regard to the characterization of viscosity property. To this end, we carried out a series of simple relaxation tests at different stretch levels. In this course, similar to the multi-step relaxation tests (Fig. 5), a strain rate of 0.5/s followed by a hold time of 10 min was used in all the tests described in this section.

Figure 7 shows the stress histories obtained from the tests on Specimen-I at 0.7 stretch level and Specimen-II at 0.5 stretch level. In Specimen-I, a rapid stress relaxation feature is displayed in the first 2 min. of hold time after which it approaches asymptotically towards an equilibrium state within next 2 min. The total magnitude of stress relaxation of Specimen-II was found much lower than that of the other specimen. This observation conforms to the viscous domain characteristics of the material as mentioned in Section 2.5. In both specimens, however, the stress relaxation characteristic was not found to vary with the change of stretch levels of the simple relaxation tests.

3. Constitutive model

The experimental observation summarized in Section 2 revealed the strain rate dependency of the materials. Typically the hyperelasticity laws are used to model elastomer response at a particular strain rate[7]. However, in order to model the rate dependency, the hyperelasticity laws are required to be combined with a rate-dependent model through a finite deformation model structure. Such model structure contains the parameters representing the equilibrium and instantaneous states, and viscosity of the material. The following sections summarize the aspects of model configuration, the approaches for hyperelasticity modeling, and incorporation of the chosen hyperelasticity law into the finite deformation rate-dependent model.

3.1 Model configuration

A three-parameter parallel model as illustrated in Fig. 8 was considered. Although the linear spring elements are used in the standard three-parameter model for linear viscoelasticity, in the present three-parameter model, a hyperelasticity model was employed to represent the nonlinear elastic behavior of each spring element. For the dash–pot element, we assume the conventional linear viscosity for simplicity. In this model, the hyperelastic element A represents the equilibrium response. The other branch consisting of hyperelastic element B and viscous dash-pot C represents the over-stress feature resulting from the rate-dependent effect. The total strain ε was decomposed into elastic strain e_e and inelastic strain e_i components.

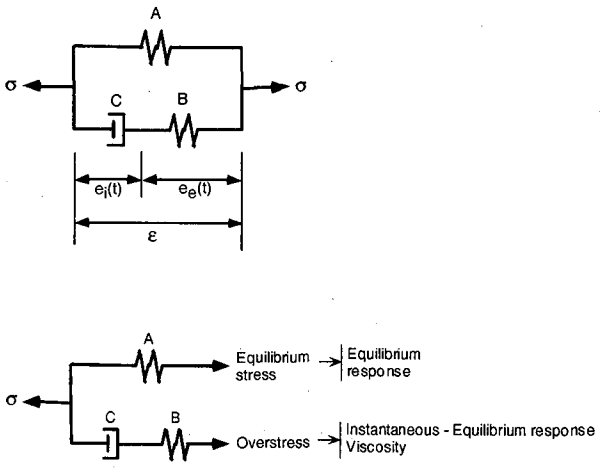

Figure 8. Three-parameter parallel model.

3.2 Hyperelasticity modeling

In hyperelasticity, under the assumption of isotropy, the stress-strain relationship is derived from a strain energy density function W[8] expressed either in terms of the strain invarients[9)-14)] or principal stretches[15)-16)]. The strain-invariant-based models are easy to implement in a mathematical formulation, while the stretch based models are more flexible in representing the experimental data particularly at higher strain levels. However, to follow a simpler computational approach, a strain-invariant-based hyperelasticity model was chosen in this study. In this approach, the three strain invariants (i.e. I, II, III) are expressed as:

$$\begin{aligned} \mathrm{I} &= \mathrm{tr}\mathbf{B} = \lambda_1^2+\lambda_2^2+\lambda_3^2, \\ \mathrm{II} &= \frac{1}{2}\left\{(\mathrm{tr}\mathbf{B})^2-\mathrm{tr}(\mathbf{BB})\right\} = (\lambda_1\lambda_2)^2+(\lambda_2\lambda_3)^2+(\lambda_3\lambda_1)^2, \\ \mathrm{III} &= \det\mathbf{B} = (\lambda_1\lambda_2\lambda_3)^2, \end{aligned} \qquad (1)$$

where $\lambda_1, \lambda_2, \lambda_3$ are the principal stretches; left Cauchy-Green deformation tensor, $\mathbf{B}=\mathbf{FF}^T$; $\mathbf{F}$=deformation gradient tensor.

Among the strain invariant based models, Mooney-Rivlin model[9),10)] is the most common one but it does not perform well at higher strain levels. To overcome this problem, a higher order function of I as proposed by Yamashita & Kawabata[14)] was incorporated in this study for modeling the responses at higher strain levels. The strain energy density function of the present model is expressed as,

$$W(\mathrm{I},\mathrm{II}) = C_5(\mathrm{I}-3)+C_2(\mathrm{II}-3)+\frac{C_3}{N+1}(\mathrm{I}-3)^{N+1}, \qquad (2)$$

where C_5, C_2, C_3, N are non-negative material constants. Here, with the parameter C_3=N=0 the function is reduced to the original Mooney-Rivlin model.

In case of uniaxial loading, under the assumption of incompressibility, the third strain invariant, III reduces to unity giving $\lambda_2=\lambda_3=(\lambda_1)^{-1}=(\lambda)^{-1}$. In such a case, the Cauchy stress in the loading direction (i.e.. σ_1) for this model is expressed as:

$$\sigma_1 = 2\left(\lambda^2-\frac{1}{\lambda}\right)\left[C_5+\frac{1}{\lambda}C_2+C_3\left(\lambda^2+\frac{2}{\lambda}-3\right)^N\right]. \qquad (3)$$

It becomes evident from equation (3) that the Cauchy stress can be decomposed into three terms associated with C_5, C_2 and C_3 coefficients. In order to clarify the individual contribution of these terms on the Cauchy stress over the tension and compression regimes, the component-wise stress-stretch functions are plotted in Fig. 9. Among these three terms, the C_2 term of the original Mooney-Rivlin Model represents the high initial stiffness of the hyperelastic response observed at low tensile strains (Fig. 9a). However, on the compression side, this term can not represent such response as observed in our experiments (Fig. 6). The C_5 term represents the large extension feature of a hyperelastic response in tension and compression regime as well (Fig. 9a). The hardening feature of the rubber molecular network[17)] follows the large extension feature (Fig. 6). The C_3 term with an exponential term N represents this high strain hardening feature (Fig. 9b). However, the effect of exponent value N on the Cauchy stress is not much sensitive. This feature of the Cauchy stress in the hyperelasticity model will be discussed once again in Section 4 in connection with the parameter identification scheme.

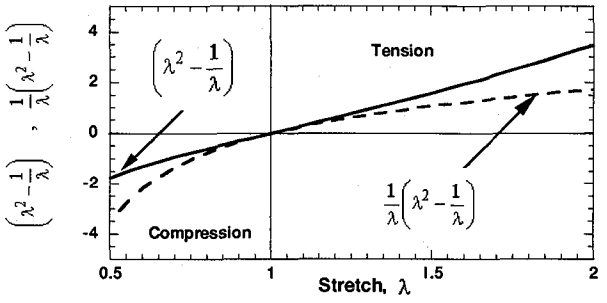

(a)

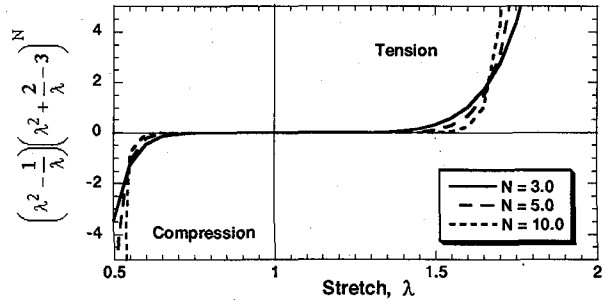

(b)

Figure 9. Cauchy stress function components. (a) C_2 and C_5 components (b) C_3 component.

3.3 Rate-dependency modeling

The stress and strain components of the three-parameter parallel model presented in Fig. 8 were converted into a finite deformation model following the formulation of Huber & Tsakmakis[2]. To do this, first we modeled each spring element (Fig. 8) in terms of hyperelasticity law and expressed the equilibrium stress, $T^{(E)}$ and overstress, $T^{(OE)}$ as follows:

$$T^{(E)} = \frac{\partial W^{(E)}}{\partial \varepsilon} \quad , \text{ for spring A} \tag{4a}$$

$$T^{(OE)} = \frac{\partial W^{(OE)}}{\partial e_e} \quad , \text{ for spring B} \tag{4b}$$

The finite deformation model was formulated under the framework of multiplicative decomposition of the deformation gradient tensor, **F**. The total deformation gradient tensor is decomposed into $\mathbf{F} = \mathbf{F}_e\mathbf{F}_i$; where $\mathbf{F}_e$ and $\mathbf{F}_i$ are the deformation gradients associated with e_e and e_i respectively. Here the $\mathbf{F}_i$ component introduces an intermediate equilibrium configuration. Such configuration is resulted when the stress is unloaded at an infinitely fast rate to an equilibrium state, provided the value of $\mathbf{F}_i$ is fixed during unloading process. Such unloading process is local, hence, neither $\mathbf{F}_e$ nor $\mathbf{F}_i$ components need to satisfy global compatibility conditions. This leads the expression of the Cauchy stress tensor **T** and rate of left Cauchy-Green deformation tensor **B** as follows:

$$\mathbf{T} = -p\mathbf{1} + \mathbf{T}_E \tag{5a}$$

$$\mathbf{T}_E = \mathbf{T}_E^{(E)} + \mathbf{T}_E^{(OE)} \tag{5b}$$

$$\mathbf{T}_E^{(E)} = 2\frac{\partial W^{(E)}}{\partial \mathbf{I}_\mathbf{B}}\mathbf{B} - 2\frac{\partial W^{(E)}}{\partial \mathbf{II}_\mathbf{B}}\mathbf{B}^{-1} \tag{5c}$$

$$\mathbf{T}_E^{(OE)} = 2\frac{\partial W^{(OE)}}{\partial \mathbf{I}_{\mathbf{Be}}}\mathbf{B}_e - 2\frac{\partial W^{(OE)}}{\partial \mathbf{II}_{\mathbf{Be}}}\mathbf{B}_e^{-1} \tag{5d}$$

$$\dot{\mathbf{B}}_e = \mathbf{B}_e\mathbf{L}^T + \mathbf{L}\mathbf{B}_e - \frac{2}{\eta}\mathbf{B}_e\left(\mathbf{T}_E - \mathbf{T}_E^{(E)}\right)^D \tag{5e}$$

where p is the hydrostatic pressure of **T** and sub-script 'E' denotes the extra part of corresponding stress tensor. **1** is the identity tensor. The subscript 'e' denotes the quantities related to $\mathbf{F}_e$. **L** is the velocity gradient tensor. Superscript 'D' denotes the deviatoric part of stress. η is the viscosity of the dash-pot. In deriving the explicit expressions for **T** and rate of $\mathbf{B}_e$, the hyperelasticity function presented in equation (2) was used together with equation (5). Equation (6) presents the final form of the **T** and the rate of $\mathbf{B}_e$.

$$\mathbf{T} = -p\mathbf{1} + 2C_5^{(E)}\mathbf{B} + 2C_3^{(E)}(\mathbf{I}_\mathbf{B} - 3)^{N^{(E)}}\mathbf{B} - 2C_2^{(E)}\mathbf{B}^{-1} + 2C_5^{(OE)}\mathbf{B}_e + 2C_3^{(OE)}(\mathbf{I}_\mathbf{B} - 3)^{N^{(OE)}}\mathbf{B}_e - 2C_2^{(OE)}\mathbf{B}_e^{-1} \tag{6a}$$

$$\dot{\mathbf{B}}_e = \mathbf{B}_e\mathbf{L}^T + \mathbf{L}\mathbf{B}_e - \frac{4}{\eta}\mathbf{B}_e\left(C_5^{(OE)}\mathbf{B}_e + C_3^{(OE)}(\mathbf{I}_\mathbf{B} - 3)^{N^{(OE)}}\mathbf{B}_e - C_2^{(OE)}\mathbf{B}_e^{-1}\right)^D \tag{6b}$$

The material parameters of the proposed model expressed in equation (6) are summarized in Table 1.

Table 1. Material parameters

Response components	Material Parameters			
Equilibrium stress	$C_5^{(E)}$	$C_3^{(E)}$	$C_2^{(E)}$	$N^{(E)}$
Overstress	$C_5^{(OE)}$	$C_3^{(OE)}$	$C_2^{(OE)}$	$N^{(OE)}$
Viscosity	η			

4. Parameter identification

On the basis of experimental observations and the constitutive model described in Section 2 and Section 3 respectively, the following sections present the parameter determination procedure for representing the equilibrium response, the instantaneous response, and the viscosity.

4.1 Equilibrium response

The coefficients of the hyperelasticity model for the equilibrium locus obtained from the multi-step relaxation tests (Sec. 2.4) were determined by the least square method. In this work, we performed our experiments in the compression regime where the C_2 term is ineffective in representing the experimentally observed high initial stiffness as discussed in Section 3.2. Hence to avoid getting negative values in the least square procedure, C_2 was assigned to zero. The values of the parameters are listed in Tables 2 and 3 for Specimen-I and II, respectively.

Table 2. Elastic material parameters (Specimen-I)

Responses	C_5	C_3	C_2	N
	MPa	MPa	MPa	
Equilibrium	0.48	0.015	0.00	3.30
Instantaneous	0.85	0.120	0.00	3.30

Table 3. Elastic material parameters (Specimen-II)

Responses	C_5	C_3	C_2	N
	MPa	MPa	MPa	
Equilibrium	0.44	0.001	0.00	3.50
Instantaneous	0.55	0.004	0.00	3.50

4.2 Instantaneous response

The monotonic compression tests presented in Section 2.5 displayed a diminishing trend in the increase of the stress response at higher strain rates indicating the approach of the instantaneous state. Interestingly, the overall stress-stretch response at each strain rate has a characteristic 'S' shaped curve, which can be described by the hyperelasticity model.

On the basis of this feature, the constants, i.e. C_5 and C_3 were determined for each monotonic compression test with different strain rates ranging from 0.001/s to 0.96/s. In the Cauchy stress-stretch relation of the hyperelasticity model (eq. (3)), the contribution from the third term is related to two parameters, i.e. C_3 and N. However, the plot of this term as presented in Fig. 9b clarifies weak sensitivity of N value to the relation. On this basis, a constant value of N as determined from the equilibrium locus of each material was used for determining C_3 parameter. The C_5 and C_3 parameters determined by this way are plotted respectively in Figs. 10 and 11 against the corresponding strain rate values for both specimens.

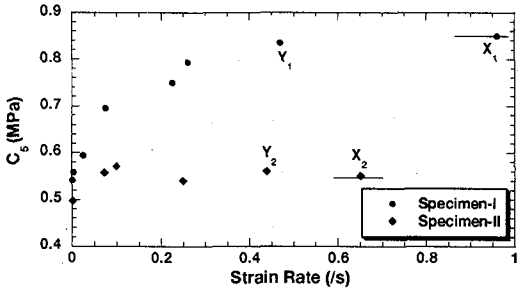

Figure 10. Best-fit C_5 values for monotonic compression tests with different strain rates.

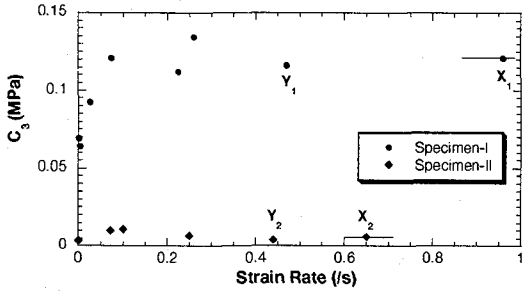

Figure 11. Best-fit C_3 values for monotonic compression tests with different strain rates.

It is interesting to note that the values of C_5 and C_3 parameters (Figs. 10 and 11) follow an asymptotic trend with the increase of applied strain rate. This must be due to approach of the instantaneous state. In case of Specimen-I such feature is noticed over a strain rate of 0.25/s, while in Specimen-II the corresponding strain rate is 0.1/s. The parameters for the instantaneous response are estimated from this asymptotic trend within finite strain rate region. The values obtained from the highest strain rate case in each specimen and denoted by X_1 and X_2 (Figs. 10 and 11) were taken for representing the instantaneous response. The values have been presented in Tables 2 and 3. The subtraction of the values of C_5, C_3, C_2 from the instantaneous to the equilibrium state gives the parameter values for the overstress response mentioned in Table 1.

4.3 Viscosity

After determining the elastic parameters for both instantaneous and equilibrium responses, the only remaining unknown one is the viscosity, η (Fig. 8). Here, simple relaxation test data was used to obtain η through simulation trials of the rate-dependent hyperelasticity model (Sec. 3.3) by comparing the computed results with experimental data.

For the relaxation test with a stretch at 0.7 in Specimen-I, η=1.125 MPa-s was found to represent the relaxation feature adequately (Fig. 12a). In Specimen-II, the corresponding value was 3.50 MPa-s (Fig. 12b).

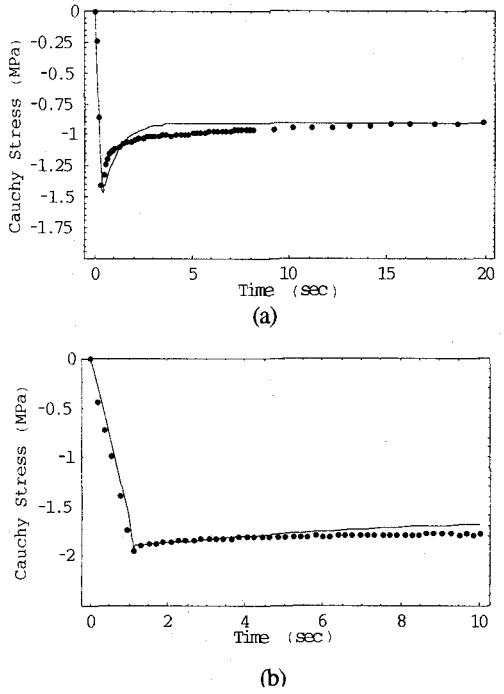

Figure 12. Estimation of viscosity parameter by simulating the simple relaxation test result; (-) Numerical simulation, (•) Experiment. (a) Specimen-I, (b) Specimen-II.

5. Verification and discussion

The determination of the viscosity parameter presented in Section 4.3 completes the parameter identification scheme. At this stage, the parameters determined in Section 4 were used in the constitutive model to verify the adequacy of the proposed scheme. In this context, Section 5.1 compares the simulation results with monotonic compression test data. In addition, Section 5.2 presents the results from a sensitivity study and discusses the asymptotic convergence of the instantaneous response with increasing strain rate observed in Section 4.2.

5.1 Comparison of simulation results with monotonic compression tests

The elastic and viscous parameters determined in Section 4 were used in the constitutive model presented in Section 3 to simulate the monotonic compression test at varied strain rates. Figs. 13 and 14 show the simulation results in comparison with experimental data for both specimens, where a good conformity is observed in all the cases. However, in case of Specimen-I, as expected, the representation of stress-stretch response at low strain levels is a bit poor (Fig. 13) particularly for lower strain rate cases due to the limitation of hyperelastic model in that region (Fig. 9a).

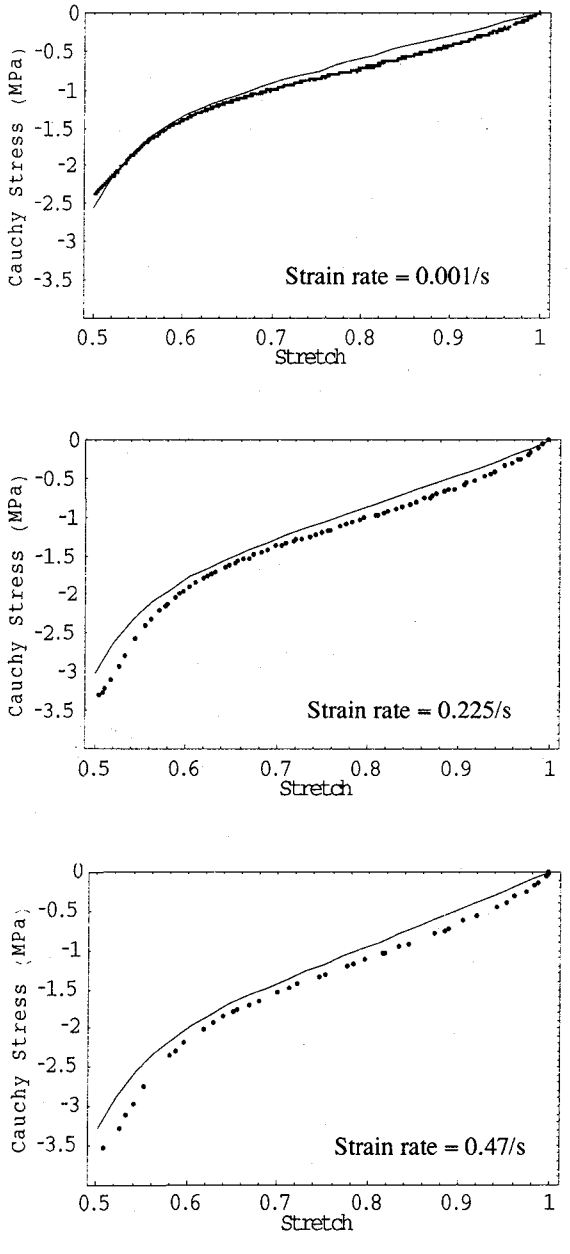

Figure 13. Numerical simulation of monotonic compression test at different strain rates for Specimen-I (-) Numerical simulation, (•) Experiment.

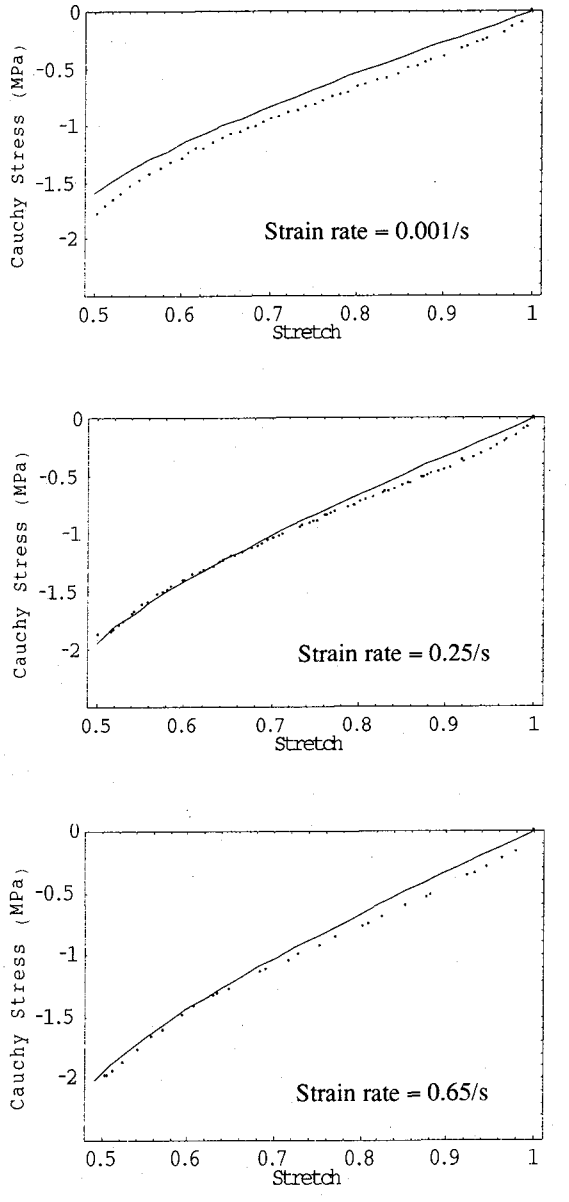

Figure 14. Numerical simulation of monotonic compression test at different strain rates for Specimen-II; (-) Numerical simulation, (•) Experiment.

In Specimen-II, the simulation result at 0.001/s strain rate is slightly poorer than other faster strain rate cases (Fig. 14). Such performance might be related to the limitation of present viscosity modeling where only one relaxation rate can be modeled in contrast to the experimental observation presented in Fig. 7b where the co-existence of two relaxation rates was detected (Section 2.6). In this case, the viscosity parameter was estimated in Section 4.3 to represent the faster relaxation rate that completes the major part of total stress relaxation within first 10 sec of the stress history (Fig. 12b). In contrast to this, the time history duration of monotonic compression test at 0.001/s up to 0.5 stretch level is 500 sec. This is much longer than the duration of relaxation stress history (10 sec) modeled by that single viscosity parameter. However, in Specimen-I, the effect of multiple relaxation

rates on the simulation result is not so prominent. Apart from these aspects, in a general trend, the numerical results slightly underestimated the response in all strain rate cases for both specimens.

5.2 Sensitivity study

In determining elastic parameters, the proposed scheme requires only one test for equilibrium response in contrast to the case of instantaneous response, where the required number of experiment is a bit large. In addition, a large number of monotonic compression experiments from slower to faster rates were carried out in this study to clarify the convergence of the hyperelasticity parameters to the asymptotic value with increasing strain rate. However, the values of C_5 and C_3 determined at different strain rates (Figs. 10 and 11) indicate the possibility of reducing the strain rate in approximating instantaneous response for practical application. Hence, at this stage, the effect of using instantaneous state parameter values estimated from different but slower strain rate cases on the simulation results was studied through a sensitivity study. The study was carried out with a view to checking the robustness of the proposed scheme and thereby to investigate the possibility of using a reduced strain rate for estimating instantaneous response parameters. To do this, in the case of Specimen-I, we take the value of one of the parameters C_5 and C_3 for the instantaneous response from the strain rate case of Y_1 (Figs. 10 and 11) while taking the other parameter from the X_1 case. The resulting errors in stress prediction occurring due to this parametric variation are presented as a function of stretch in Fig. 15 where,

$$\text{Error}(\%) = \frac{\sigma_X - \sigma_Y}{\sigma_X} \times 100 \qquad (7)$$

Simulation of monotonic compression tests at three different strain rates were considered. In case of Specimen-II, a similar study was carried out for X_2 and Y_2 cases (Figs. 10 and 11) and the corresponding results are plotted in Fig. 16.

In Specimen-I, the considered reduction of strain rate from X_1 to Y_1 is 51% while in Specimen-II, the corresponding shift is 31%. In contrast to such large reduction of strain rate in selecting instantaneous parameters, the errors in stress prediction remain within 2% in both specimens as revealed from Figs. 15 and 16. This confirms the robustness of the proposed instantaneous state identification scheme and opens the scope of reducing the strain rate for practical application. A detail look over the Figs. 15 and 16 shows that the effect of C_5 parameter variation was dominant over the entire stretch range in contrast to that of the C_3 parameter that was only visible at high strain levels. In general, a reverse trend was also observed between these two effects. Such observations can readily be explained from the role of each of these parameters at different stretch levels as presented in Fig. 9 and discussed in Section 3.2. Apart from these aspects, the effect of strain rate on C_3 parameter was found to be insignificant.

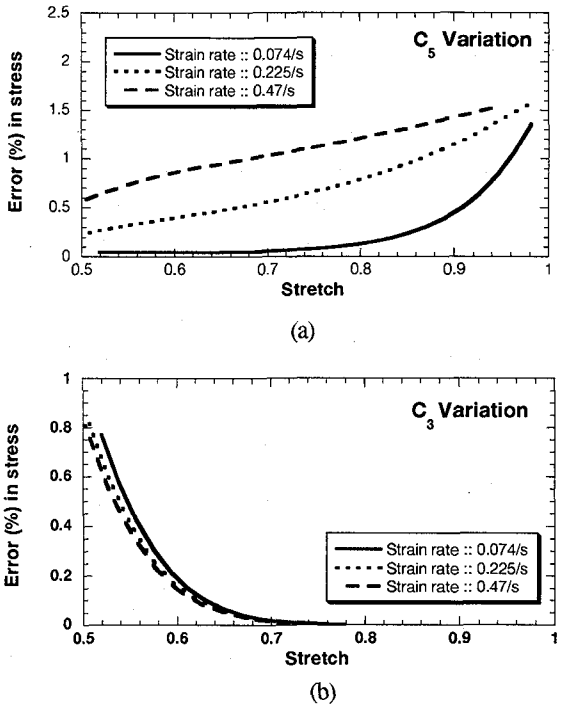

Figure 15. Effect of instantaneous response parameter variation on stress in monotonic compression test for Specimen-I ; (a) C_5 parameter, (b) C_3 parameter.

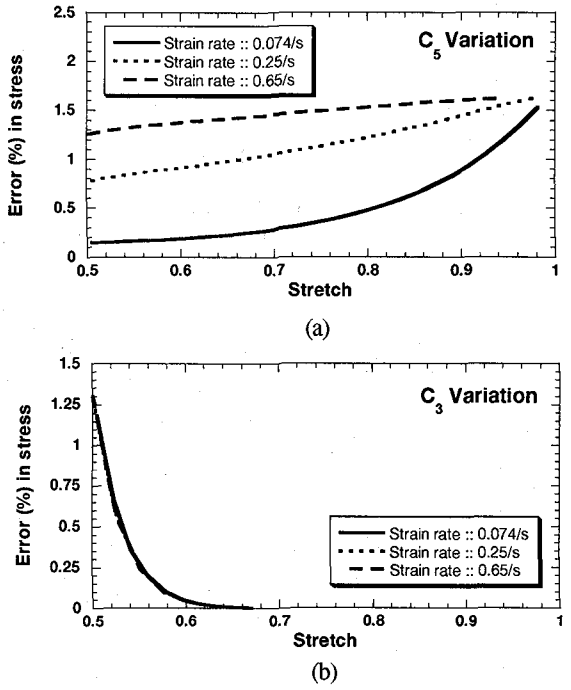

Figure 16. Effect of instantaneous response parameter variation on stress in monotonic compression test for Specimen-II ; (a) C_5 parameter, (b) C_3 parameter.

6. Conclusions and further remarks

1) The equilibrium response of elastomers can be approximated from a multi-step relaxation test.

2) The instantaneous response can be estimated from a series of constant-rate monotonic compression tests at different strain rates.

3) The hyperelasticity model can be used to find out the parameters for the equilibrium and instantaneous responses from the tests mentioned in (1) and (2). In this connection, incorporation of an exponential term as proposed by Yamashita & Kawabata[14] in the strain energy density formulation was found to improve the stress-stretch representation at higher stretch level.

4) When the elastic parameters of the material are known, the rate-dependent finite deformation hyperelasticity model can be used to find out the viscosity parameter by comparing the simple relaxation test data.

5) The comparison of numerical results with monotonic compression test results for different strain rate cases has shown the adequacy of the proposed procedure. However, in case of modeling any elastomer with more than one prominent relaxation rates, the numerical model presented in this paper needs some improvement.

6) A sensitivity study has shown the possibility of reducing the strain rate of monotonic compression experiments for estimating the instantaneous response for practical applications. This also displayed the robustness of the proposed procedure.

7) In this paper, we have investigated the nonlinear viscoelastic response of elastomers in compression side and proposed an experimental scheme to identify the parameters in a physically meaningful way using a rate-dependent constitutive model. Conceptually, the proposed experimental outline and subsequent parameter identification procedure are applicable in predicting the viscoelastic response of elastomers in tension regime as well. To this end, it is of the coming up interest of the authors to check the performance of the scheme on tension side.

Acknowledgement

The authors are indeed grateful to Professor H. Horii, Associate Professor M. Abe and Mr. J. Yoshida, Department of Civil Engineering, University of Tokyo, Tokyo, Japan for their valuable comments and suggestions at various stages of the work. The authors are particularly grateful to Professor H. Horii for extending experimental facilities of his laboratory to carry out the mechanical tests of the investigation. The technical assistance provided by T. Matsuo, Department of Civil and Environmental Engineering, Saitama University, Japan is also gratefully acknowledged. The authors gratefully acknowledge the kind cooperation extended by the Yokohama Rubber Co. by providing test specimens. This research was partly financed by Grant-in-Aid for Scientific Research (C) (No. 12650457) from the Japanese Ministry of Education, Science, Sports and Culture.

References

1) Kelly, J. M., *Earthquake Resistant Design with Rubber*, Springer-Verlag, London, 1997.

2) Huber, N. and Tsakmakis, C., Finite deformation viscoelasticity laws, *Mech. Mater.*, 32, pp.1-18, 2000.

3) Lion, A.., A constitutive model for carbon black filled rubber: Experimental investigations and mathematical representation, *Continuum Mech. Thermodyn.*, 8, pp. 153-169, 1996.

4) Miehe, C. and Keck, J., Superimposed finite elastic-viscoelastic-plastoelastic stress response with damage in filled rubbery polymers. Experiments, modeling and algorithmic implementation, *J. Mech. Phys. Solids*, 48, pp. 323-365, 2000.

5) Mullins, L., Softening of rubber by deformations, *Rubber Chem. Technol.*, 42, pp. 339-362, 1969.

6) Bueche, F., Mullins effect and rubber-filler interaction, *J. Appl. Polym. Sci.*, 5(15), pp. 271-281, 1961.

7) Bonet, J. and Wood, R. D., *Nonlinear Continuum Mechanics for Finite Element Analysis*, Cambridge University Press, Cambridge, 1997.

8) Charlton, D. J., Yang, J. and Teh, K. K., A review of methods to characterize rubber elastic behavior for use in finite element analysis, *Rubber Chem. Technol.*, 67, pp. 481-503, 1993.

9) Mooney, M., A theory of large elastic deformation, *J. Appl. Phys.*, 11, pp. 582-592, 1940.

10) Rivlin, R. S. and Saunders, D. W., Large elastic deformations of isotropic materials VII. Experiments on the deformation of rubber, *Phil. Trans. Roy. Soc.* 243, pp. 251-288, 1951.

11) Hart-Smith, L. J., Elasticity parameters for finite deformations of rubber-like materials, *Z. Angew. Math. Phys.* 17, pp. 608-626, 1966.

12) Alexander, H., A constitutive relation for rubber-like materials, *Int. J. Engng. Sci.*, 6, pp. 549-563, 1968.

13) James, A. G., Green, A. and Simpson, G. M., Strain energy functions of rubber. I. Characterization of gum vulcanizates, *J. Appl. Polym. Sci.*, 19, pp. 2033-2058, 1975.

14) Yamashita, Y. and Kawabata, S., Approximated form of the strain energy density function of carbon-black filled rubbers for industrial applications, *J. Soc. Rubber Ind. (Jpn)*, 65(9), pp. 517-528, 1992. (in Japanese).

15) Valanis, K. C. and Landel, R. F., The strain-energy density function of a hyperelastic material in terms of the extension ratios, *J. Appl. Phys.*, 38(7), pp. 2997-3002, 1967.
16) Ogden, R. W., *Non-linear Elastic Deformations*, Ellis Horwood Ltd., Chichester, 1984.
17) Treloar, L. R. G., Stress-strain data for vulcanised rubber under various types of deformation, *Trans. Farady Soc.*, 40, pp. 59-70, 1944.

(Received on September 14, 2000)